Original Article

In vitro investigation of contrast flow jet timing in patient-specific intracranial aneurysms

Liang-der Jou, Virendra R. Desai, Garvin W. Britz

Department of Neurosurgery, Houston Methodist Hospital, Houston, Texas 77030, USA

Correspondence to: Liang-der Jou, PhD. Scurlock Tower, Suite 944, Department of Neurosurgery, Houston Methodist Hospital, Houston, Texas 77030, USA. Email: ljou@houstonmethodist.org.

Background: The direction and magnitude of intra-aneurysmal flow jet are significant risk factors of subarachnoid hemorrhage, and the change of flow jet during an endovascular procedure has been used for prediction of aneurysm occlusion or whether an additional flow diverter (FD) is warranted. However, evaluation of flow jets is often unreliable due to a large variation of flow jet on the digital subtraction angiograms, and this flow pattern variation may result in incorrect clinical diagnosis Therefore, factors contributing to the variation in flow jet are examined at an *in vitro* setting, and the findings can help us to understand the nature of flow jet and devise a better plan to quantify the aneurysmal hemodynamics accurately.

Methods: Intra-aneurysmal flows in three patient-specific aneurysms between 11 and 25 mm were investigated in vitro, and a FD was deployed in each aneurysm model. X-ray imaging of these models were performed at injection rates between 0.2 and 2 mL/s. Pulsatile blood pump and aneurysm model were imaged together to determine the timing of flow jet.

Results: The contrast bolus arrives at the aneurysm early at high contrast injection rates. The flow patterns with slow injection rates exhibit strong inertia that is associated with the systole flow. Flow jets arrive at the aneurysms at the peak systole when the bolus is injected at 0.2 mL/s. The contrast-to-signal ratio is the highest at the injection rate of 0.5 mL/s. Effect of flow diversion can only be assessed at an injection rate greater than 0.5 mL/s.

Conclusions: Intra-aneurysmal flow jet is highly dependent on the injection rate of the contrast agent. For the internal carotid artery (ICA) aneurysms, the systolic flows can be visualized at slow injection rates (<0.5 mL/s), while the diastolic flow jets are visible at higher injection rates (>1 mL/s). Dependence of flow jet on the contrast injection rate has serious clinical implications and needs to be considered during diagnostic procedures; a protocol with a consistent injection rate is highly recommended.

Keywords: Digital subtraction angiography (DSA); stent; hemodynamics; intracranial aneurysms; subarachnoid hemorrhage

Submitted Jan 15, 2016. Accepted for publication Feb 25, 2016.
doi: 10.21037/qims.2016.03.06
View this article at: http://dx.doi.org/10.21037/qims.2016.03.06

Introduction

Vessel wall weakened by hemodynamic stresses, followed by further degeneration and degradation, is one of the major risk factors that are responsible for initiation and rupture of intracranial aneurysms (1-3). The direction and magnitude of intra-aneurysmal flow jet are significant hemodynamic risk indicators of subarachnoid hemorrhage. Flow diverter (FD) has become an attractive alternative for management of unruptured intracranial aneurysms (4); a FD reconstructs the parent artery and stimulates thrombus within the aneurysm (5). Presence of FD also redirects the

intra-aneurysmal flow, reduces hemodynamic stresses on the aneurysmal wall, and lowers rupture risk (6). Reports on the short- and long-term outcome of these devices are encouraging (7-9).

After flow diversion, the aneurysm is often not thrombosed immediately and the rupture risk remains until its complete occlusion. Therefore, it is critical to assess the quality of flow diversion during an interventional procedure, either by the presence of contrast stasis or by change of flow jets. Contrast accumulation within an aneurysm results from slower washout of contrast agent, and presence of contrast stasis is regarded as the first sign of flow diversion. Grunwald *et al*. have suggested an angiographic grading scheme for post-procedural occlusion evaluation based on the level of residual contrast filling (10). Using an optical flow technique, Pereira *et al*. proposed a "MAFA" (mean aneurysm flow amplitude) factor to determine the change of flow jet during digital subtraction angiography (DSA) (11). Several other variables, such as diffusion and convection relaxation times, have also been used for quantification of flow diversion (12). These DSA-based techniques provide a convenient way to assess the effect of flow diversion during an endovascular procedure, and most of them require a bolus of contrast injection (13), with an extended period of imaging (12) and/or at higher DSA frame rate (11,13,14).

The pattern of contrast influx is often altered after deployment of a FD, and changes of both flow direction and velocity are visible immediately on the DSA. Since flow pattern is postulated for its possible role in aneurysm rupture (15), modification of flow pattern indicates a change of rupture risk. The qualitative evaluation of flow jets, however, is unreliable due to a great variation of flow jet appearance on the DSA. Nevertheless, the flow jet variation has never been examined mostly because of the nature of *in vivo* environment where variables could not be controlled.

In fact, contrast injection introduces X-ray signal modulation that is useful for hemodynamic assessment of blood flow in arteries and intracranial aneurysms (13). The hyper-intense signal on the DSA is associated with the diastole flow during which the contrast agent is less diluted by blood (14). The contrast agent is diluted considerably during the systole and produces a lower signal. Because of a strong correlation between the rupture risk and high pressure/large flow impact at the systole, we investigate the timing of flow jet quantitatively and examine the possibility to visualize systolic flows in intracranial aneurysms at an *in vitro* setting.

Materials and methods

Three rigid transparent patient-specific aneurysm models, based on 3D rotational angiography (RA) images at the resolution of 0.15 mm, were made using stereolithography (Protogenic; Lakewood, CO, USA), similar to the technique in Tateshima *et al*. (16). The aneurysm geometry was obtained by segmentation of 3D images and a 2-mm thick wall was added to the geometry. The final model was a shell that represented the arterial lumen, but the aneurysm wall was encased in a clear block to eliminate light reflection and provide better visualization of the device (*Figure 1A*).

These unruptured saccular aneurysms were selected for their sizes (>10 mm) that could provide a reasonable area for imaging. Aneurysm A was an 11-mm posterior communicating aneurysm in a 76-year-old female patient, aneurysm B was a 25-mm aneurysm located at the supraclinoid segment of the internal carotid artery (ICA) in a 66-year-old female patient, and aneurysm C was a 12-mm middle cerebral artery (MCA) aneurysm in a 78-year-old female patient. The protocol was approved at our institution before the study began. Each model included the petrous segment of the ICA and extended to the anterior cerebral artery (ACA) and MCA. The wall thicknesses of these rigid models were not considered because the current focus was on the angiographic behavior during contrast injection; nevertheless, a compliant model may influence the flow pattern in the aneurysm.

Two identical copies were made for each aneurysm; one of them was used for imaging of FD, and the other copy as the control. One pipeline embolization device (PED) (Covidien, Dublin, Ireland), a braided stent with 48 wires, was placed in each model, 4 mm × 18 mm for aneurysm A, 3.5 mm × 18 mm for aneurysm B, and 2.5 mm × 18 mm for aneurysm C. Thus, these devices had the same length (18 mm), but varied in the diameter. A picture of the PED for aneurysm A is in *Figure 1A*. The dimensions of these devices were the same as those for treatment of these patients. All these aneurysms exhibited some contrast stasis after flow diversion.

Each of these models was connected to a flow loop powered by two flow pumps in parallel, one steady flow pump (United Biologics; Tustin, CA, USA) and one pulsatile flow pump (Harvard Apparatus; Road Holliston, MA, USA). The setup was similar to Tsai and Savas (17) where the steady flow pump provided a low steady component that the pulsatile flow pump lacked. The entire flow system was pressurized and driven by these pumps, and no additional

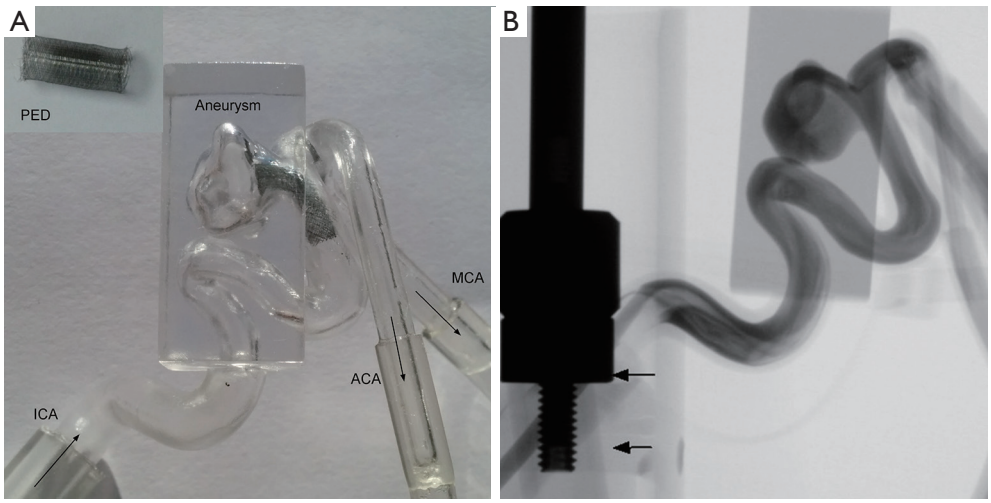

Figure 1 Image of the setup (pump and piston) and aneurysm model. (A) Aneurysm model A constructed from the 3D RA images with a device deployed across the aneurysm neck, and the PED in inset. The flow directions are indicated by arrows. The ICA is attached to the pumps, while the MCA and ACA are connected to the reservoir; (B) the piston is imaged with the phantom together so the timing of pump cycle can be determined. Arrows indicate the highest and lowest positions of the piston, and the distance between them is proportional to the stroke volume. These two positions corresponds to t=0.75 and 1.25 in *Figure 2*, respectively, and t=1 is at the peak systole. RA, rotational angiography; PED, pipeline embolization device; ICA, internal carotid artery; MCA, middle cerebral artery; ACA, anterior cerebral artery.

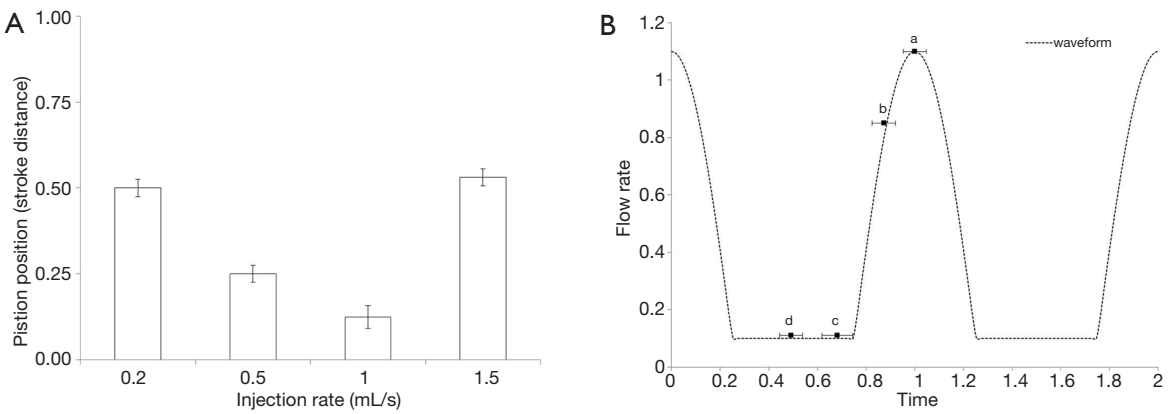

Figure 2 The phases of piston motion that produce the contrast jet. (A) The piston location at the time of contrast jet arrival for aneurysms A and B at four different injection rates; (B) the phases of piston motion producing the jet relative to the flow cycle. (a) 0.2 mL/s, (b) 0.5 mL/s, (c) 1 mL/s, and (d) 1.5 mL/s. Time is normalized by the pump cycle time. The error bars indicate the range of flow jet arrival time.

pressure source was applied as the baseline. Our flow simulation showed that the baseline pressure did not affect the flow rate or flow diversion in a flow rate-driven system. The same flow rate, equivalent to 4 mL/s, was provided by the pumps at the entrance of the ICA for all three cases. The actual flow rate at the MCA for aneurysm C was lower due to the ICA bifurcation. The piston of the unsteady flow pump was placed within the X-ray field of view (FOV), and the piston motion was captured for determination of the pump cycle (in *Figure 1B*). This approach circumvented technical issues related to synchronization of the X-ray imaging with flow pumps.

The medium in the flow loop was replenished after each contrast injection to avoid accumulation of contrast agent in the system, and contamination of the fluid by contrast agent could lead to higher viscosity and sluggish flow near

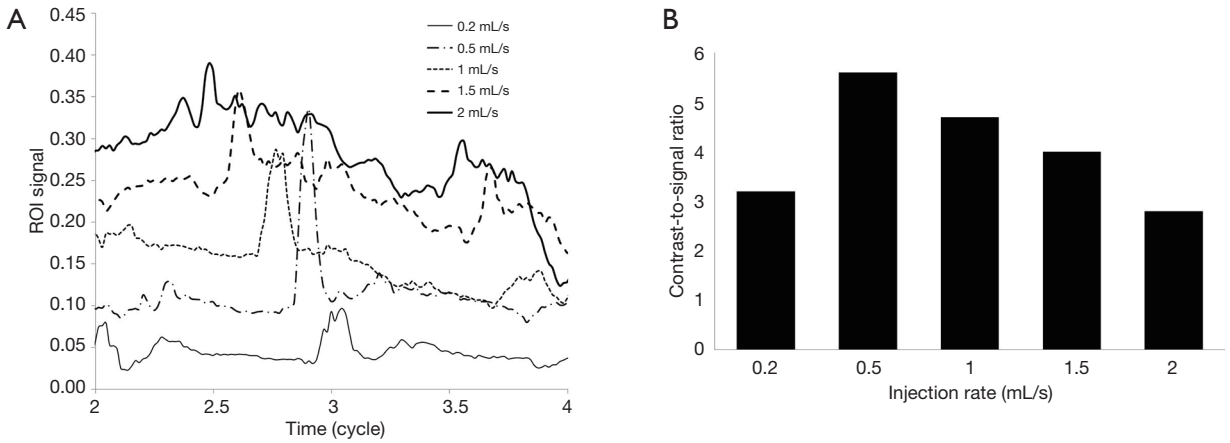

Figure 3 The X-ray signals of an ROI and contrast-to-signal ratios. (A) X-ray signals at an ROI in aneurysm B for five different injection rates. The largest peak in each case indicates the arrival of the contrast bolus; (B) contrast-to-signal ratios at the bolus.

the wall. Instead of blood mimicking fluid or heparinized blood, water was used as the medium with an additional advantage. Since the viscosity of blood was approximately four times higher than that of water, the flow rate and frequency of the pump was set four times slower so that the Reynolds number and Womersley number would match the physiological conditions. Because of the pump being four times slower, 120 frames per heart beat were acquired during imaging, equivalent to four times greater than the maximum frame rate available clinically (30 f/s). This approach overcame a technical limitation on the frame rate and improved the temporal resolution at the same time. The flow loop was connected to a mechanical injector through a straight 6 F catheter for contrast administration, and the tip of the catheter was parked at the beginning of the petrous segment. The injection rate of the contrast (Omnipaque 300; GE Healthcare) varied between 0.2 and 2 mL/s, and the duration of injection was maintained at three cardiac cycles; however, the total imaging time for each case was 20 s, the maximum duration of our system.

After images were acquired, unsubtracted images were reviewed to identify the piston motion and derive the pulsatile waveform of the flow loop. The upstroke of the piston was related to the systolic phase of the waveform. The timing of intra-aneurysmal flow jet into the aneurysm was identified on the subtracted images and the frame associated with a surge of the contrast at the aneurysm was recorded. At each run, more than one contrast jet could be observed on the subtracted images (11,14), and the second jet was used for analysis because the first jet was often truncated and incomplete. These frames marked the instant of contrast bolus arrival and the specific time of a cycle when flow impingement occurred.

Results

The X-ray signals at an ROI in aneurysm B for five different injection rates are shown in *Figure 3*. Each signal peak represents the instant when the contrast bolus arrives, and these boluses from various injection rates do not arrive at the same instant of a cycle. The contrast bolus arrives sooner at higher injection rates and later when the injection rate is lower. Therefore, our result shows that the contrast bolus does not travel with the blood, and the total flow rate in the artery during the contrast injection is greater than either the arterial flow rate or the injection rate. The contrast-to-signal ratio is defined as the signal of flow jet to the signal at the remaining aneurysm where there is little or no contrast accumulation. The contrast-to-signal ratio peaks at the injection rate of 0.5 mL/s, and is reduced by 50% at the injection rate of 2 mL/s.

Although the contrast agent cannot be injected at a specific instant of a cycle, we can learn the timing of the contrast arrival from the piston motion. Timings of bolus arrival for two ICA aneurysms (A&B) are shown in *Figure 2*, in which t=1 is associated with the peak systole. Presence of FD does not influence the timing of flow jets. *Figure 2* is essentially a plot of the relative pump position when the contrast bolus enters the aneurysm. While the piston is at a similar location for injection rates of 0.2 and 1.5 mL/s in *Figure 2A*, the former is during the upstroke and the latter at the down-stroke. The flow jet arrives at

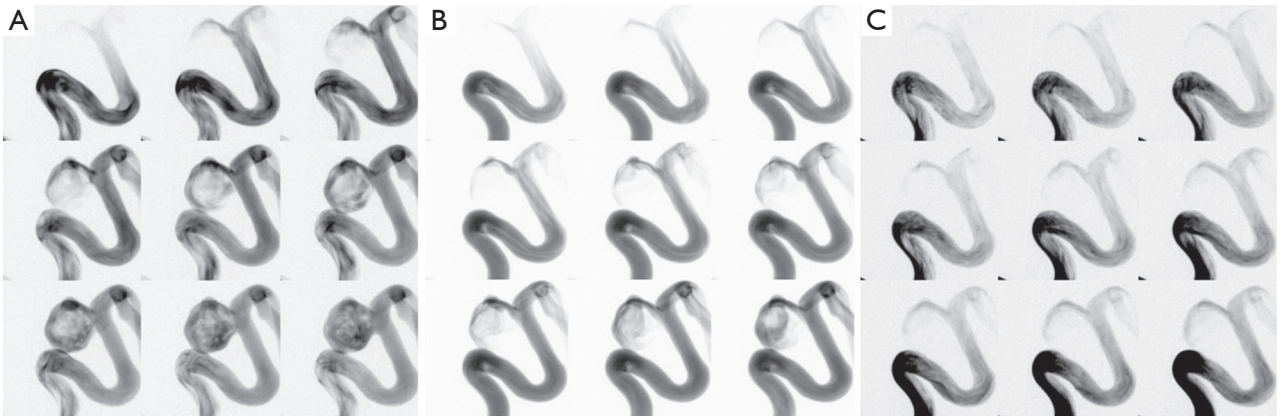

Figure 4 Nine consecutive frames of flow jet in an untreated posterior communicating artery aneurysm (aneurysm A) at three injection rates, (A) 0.5 mL/s, (B) 1 mL/s, and (C) 1.5 mL/s. Slow contrast influx is associated with high injection rates, and the arterial signal is inverse proportional to the jet speed.

the aneurysm at the peak systole when the injection rate is the lowest; at an injection rate greater than 1 mL/s, the flow jet arrives during the diastole (or when the piston is pulling back). Because the contrast boluses do not arrive at the aneurysm at the same instant of a cycle, the DSA flow patterns actually depend on the contrast injection rate. The systole flow appears on the DSA with low injection rates, and the diastole flow for high injection rates. Dependence of the DSA on the contrast injection rate may have serious implications on clinical diagnosis of flow diversion.

Figure 4 shows the flow jets in aneurysm A without a PED at three injection rates. These consecutive frames show the convective motion of the contrast bolus and demonstrate the speed of flow jet. The aneurysm is filled with the contrast faster at a slower injection rate (*Figure 4A*) than at a higher injection rate (*Figure 4C*). This counter-intuitive observation is mainly due to a higher arterial flow rate in *Figure 4A*. A stronger arterial signal in *Figure 4C* is the evidence that the flow jet exists at the diastole. *Figure 4* agrees with the phase of piston motion in *Figure 2*, and it is possible to estimate the speed of flow jet from these consecutive frames in *Figure 4*.

Before flow diversion, the flow pattern remains the same throughout the cycle (*Figure 4*); however, the contrast jet enters the aneurysm through the middle of the neck after flow diversion (*Figure 5*). The post-FD flow jet presents a faster contrast influx at the injection rate of 0.5 mL/s, but the flow jet at the injection rate of 1 mL/s, occurring during the diastole, progresses very slowly into the aneurysm.

Aneurysm B exhibits a flow entry at the distal neck before flow diversion; after flow diversion, flow jet emerges through the middle of the aneurysm neck and impinges on the dome directly (*Figure 6*), except at the injection rate of 0.2 mL/s. This shift of flow entry site indicates a reasonable flow diversion. At the highest injection rate (2 mL/s), the flow jet is hardly noticeable due to a hyperintense background signal within the aneurysm, resulting in a low contrast-to-signal ratio.

Figure 7 shows the timings of flow jet for the MCA aneurysm (aneurysm C). The pump piston is in the acceleration phase of the systole for all injection rates, and the flow jet associated with the slowest injection rate occurs at the peak systole. On the DSA in *Figure 8*, a flow jet for the slowest injection rate enters the distal neck with greatest inertia, but the flow jet shifts to the middle of the neck at higher injection rates. This finding contradicts the common belief that a flow jet through the middle of the aneurysm neck is often associated with slower intra-aneurysmal flows after FD (18). At injection rates greater than 1 mL/s, flow stasis is established immediately due to the orientation and large aspect ratio of this aneurysm. Thus, flow stasis is also injection rate dependent.

Discussion

Effect of flow diversion is currently assessed by presence of contrast stasis or change of flow pattern (10,11,19); however, they have not been very reliable in our clinical experience. Our study quantifies the timing of flow jet by imaging aneurysm phantom and flow pump together and shows that both contrast stasis and change of flow jet are injection rate dependent. Our results also demonstrate

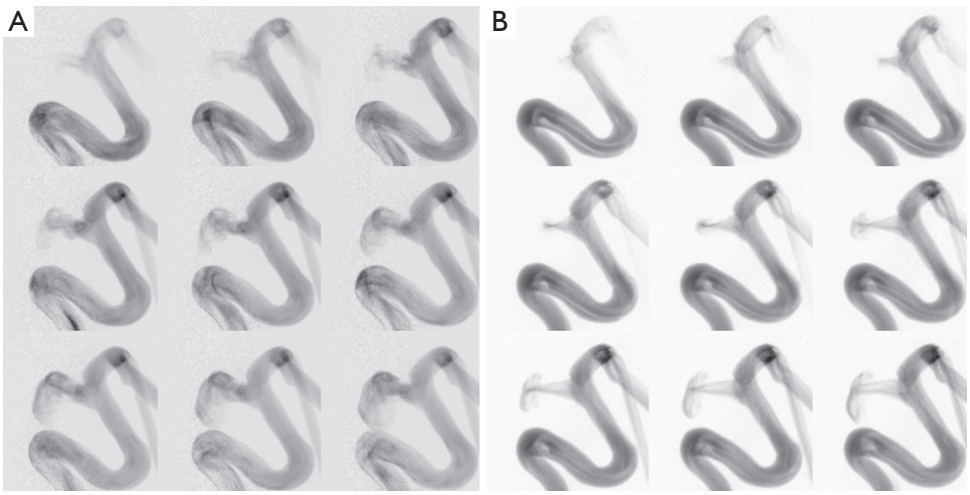

Figure 5 Nine consecutive frames of flow jet in aneurysm A with a 4 mm × 18 mm PED at injection rates of (A) 0.5 mL/s and (B) 1 mL/s. Direction of flow jet is altered only at the higher injection rate. PED, pipeline embolization device.

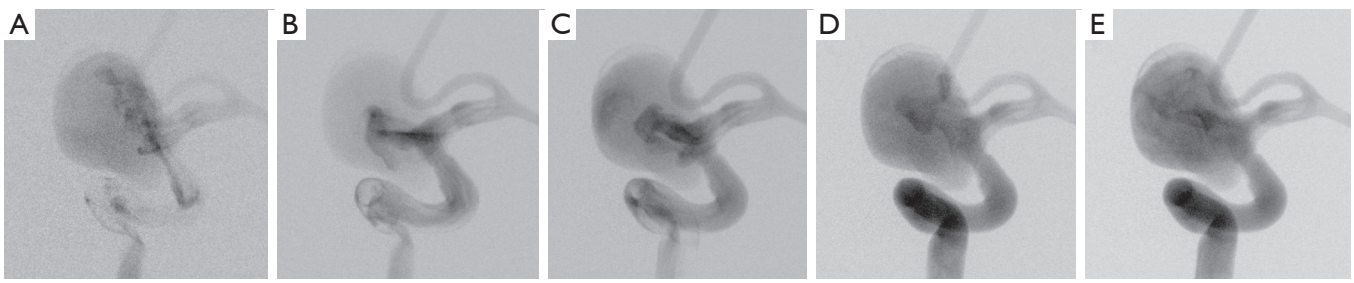

Figure 6 Flow jet in aneurysm B with a 3.5 mm × 18 mm PED at five different injection rates. (A) 0.2 mL/s, (B) 0.5 mL/s, (C) 1 mL/s, (D) 1.5 mL/s and (E) 2 mL/s. The distal jet at the slowest injection rate is associated with the systolic flow. PED, pipeline embolization device.

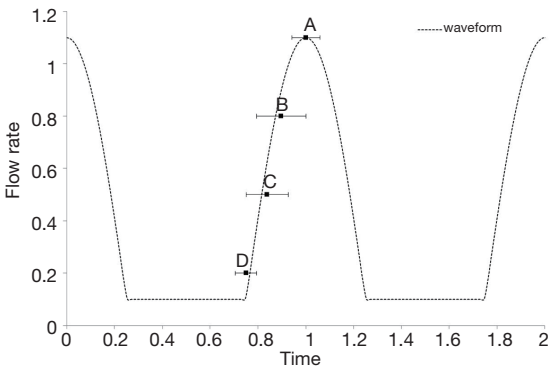

Figure 7 The arrival time of contrast bolus in terms of the phase of piston for the MCA aneurysm at four different injection rates, (A) 0.2 mL/s, (B) 0.5 mL/s, (C) 1 mL/s, and (D) 1.5 mL/s. The error bars indicate the range of flow jet arriving time. MCA, middle cerebral artery.

the possibility of visualizing systolic and diastolic flow patterns by controlling the contrast injection rate. Based on our findings, the high injection rates used previously in other studies (1.5–2 mL/s) explored only the diastolic flow for the ICA aneurysms (11,14). The systolic flow jet that contributes to elevation of wall shear stress (19) and is responsible for flow impingement has been ignored in the DSA. Flow diversion affects systolic and diastolic flows differently; the diastolic flow jet is affected by deployment of a FD, but the systolic flow jet is not amenable to FD due to its strong inertia. This fact alone may change how we perceive the flow diversion in the future.

The differences in flow pattern at various injection rates are analyzed in our *in vitro* experiments. The systolic flow jet from the slowest injection rate, often pointing to the same direction as the flow jet before flow diversion, gives

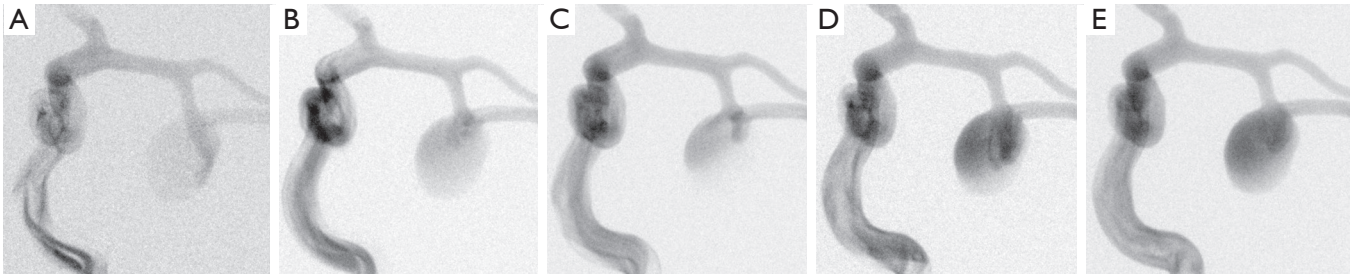

Figure 8 Flow jets in aneurysm C with a 2.5 mm × 18 mm PED at five different injection rates, (A) 0.2 mL/s, (B) 0.5 mL/s, (C) 1 mL/s, (D) 1.5 mL/s, and (E) 2 mL/s. The aneurysm is saturated with greater contrast concentration at higher injection rates (D,E). PED, pipeline embolization device.

an impression that flow diversion is less than optimal. The diastolic flow jet at higher injection rates cannot fully represent the true effect of flow diversion due to its low inertia. Clinicians favor a central flow jet with peripheral stasis, as in *Figure 6B-D* (20); this type of flow pattern is highly influenced by the inertia and appears only during the acceleration phase of the systole. A flow jet can be used for diagnosis only during this period.

Since flow jet is visible only during contrast influx, the flow pattern that presents to us is actually dictated by contrast injection. In most clinical procedures, manual contrast injection generates one contrast influx (wash-in), followed by a period of wash-out. Any treatment decision based on the contrast stasis or intra-aneurysmal flow jet needs to account for flow pattern variation within a cycle that is influenced by the contrast injection rate (21). A slow injection with a mechanical injector, as in our study, produces multiple flow jets without overwhelming the aneurysm with contrast agent or saturating the X-ray signal, and offers considerable advantages over manual injections.

A contrast bolus will arrive at the aneurysm early if it is injected at a faster rate, but it may not be apparent that a bolus of slowly injected contrast always reaches the aneurysm at the peak systole. A previous study shows that the contrast concentration is the highest at the diastole when the arterial flow rate is the lowest (14). At higher injection rates, the systolic flow with a low contrast concentration enters the aneurysm that has been enhanced by the contrast agent from previous periods so the systolic flow jet is hardly noticeable; on the other hand, the diastolic flow carrying a higher contrast concentration is easier to identify on subtracted images. This dilution effect explains why the flow jets in the ICA aneurysms occur at the diastole when the injection rate is greater than 1 mL/s. When the injection rate is less than 0.5 mL/s, dilution plays a minor role, and the bolus is driven mostly by high pressure/strong inertia during the systole. When the bolus is reaching the aneurysm neck, the aneurysm is largely unenhanced and the flow jet is easy to see even at low contrast concentration.

The same principle applies to the MCA aneurysm as well; a similar pressure/flow increase is needed for the contrast bolus to reach the aneurysm, and the acceleration during the systole offers this inertia surge. Because the flow rate at the MCA is lower than that in the ICA, the window of opportunity to visualize the flow jet is smaller. At low injection rates, the intra-aneurysmal flow is dominated by the arterial flow rate than by the contrast injection rate, and this is the reason that flow jet at low injection rates always reaches the aneurysm at the peak systole. Nevertheless, no flow jet from the deceleration phase of a cycle is observed.

The timing of flow jet is independent of the transit time or the distance between the aneurysm and tip of the catheter where the contrast injection is administrated. These three aneurysms were selected mainly for their sizes (>10 mm), and the distance between the aneurysm and catheter varies from 5.5–7.2 cm for the ICA to 9 cm for the MCA. The difference in the traveling distance (or transit time) does not change the fact that a slow contrast injection produces the systolic flow jet for all three aneurysms. Although the hardware prohibits us from synchronizing the mechanical injector with the flow pump, we can manipulate the contrast injection rate to investigate the intra-aneurysmal flow jet that is critical to our understanding of aneurysmal mechanics and rupture risk. We are uncertain at this time about the effect of injection rate on contrast stasis, but we do notice slightly more contrast stasis at lower injection rates for aneurysm A. Despite of a small number of aneurysms studied, these models should represent typical behavior of aneurysms located between the cavernous sinus and MCA bifurcation.

An injection rate of 0.2 mL/s gives a very low contrast-to-signal ratio so that it may not be suitable for *in vivo* applications; an injection rate of 0.5 mL/s produces a flow jet at the late acceleration phase of the systole with a reasonable contrast-to-signal ratio. Injection rates greater than 2 mL/s, however, do not give enough of image contrast and visualization of flow jet then becomes a challenge. Therefore, the range of contrast injection rate that provides diagnostic information is between 0.5 and 1.5 mL/s. A range of injection rates between 1.5–2 mL/s was used previously (11,14); Benz *et al*. analyzed the signal energy spectrum with a much higher injection rate (5 mL/s) (22), and Bonnefous *et al*. estimated the blood velocity in arteries from the DSA using injection rates between 1–4 mL/s (13). Most studies did not report how fast the contrast bolus was administered or whether a mechanical injector has been used.

Contrast injection can be simulated numerically using computational fluid dynamics (CFD). Flow jets on the DSA are the streak lines of dyes, different from the streamlines presented in most CFD studies. In most virtual angiography studies, contrast administration is not explicitly modeled, and the contrast agent is moving with the blood and is not mixed with the blood flow in the parent artery (20,23,24). Thus, simulated contrast influx reflects the original blood flow pattern and cannot validate the timing of flow jet observed in our study. *In vivo* validation that requires synchronizing imaging with heart beats would be challenging so our *in vitro* setup is a good option to examine the flow jet at various phases of a cycle.

For clinical diagnosis, a mechanical injector is required and the DSA images based on manual injection are not reliable. Flow jet is highly dependent on the local anatomy and injection rate of contrast agent, and appearance of variable flow jet may lead to erroneous interpretation of flow diversion and unnecessary intervention. Second, the injection rate needs to be consistent and is recommended to be between 0.5 and 1 mL/s. A comparison of two images acquired at different instants of a cycle will not provide meaningful information for quantification assessment. This is in contrast to our current clinical practice that seeks directional change of flow jet and favors flow stasis. Flow jet at the peak systole is often strong and not amenable to change; an inability to produce anticipated flow jet diversion at slow injection rates does not preclude the possibility that therapeutic effect has been achieved and additional interventions is not needed. However, the unyielding flow jet at high injection rates may warrant further attention.

Our study is limited by the waveform produced by our mechanical pumps. The steady component during the diastole prevents the retrograde flow during the down stroke of the pulsatile flow pump, and it does not capture the feature of a physiological carotid waveform. In order to improve the temporal resolution from 30 to 120 f/s, water is used in the current study. A mixture of water (or water-glycerol solution) and contrast medium has a viscosity different from that of the blood (25). This change of viscosity due to contrast injection has not been considered even though the original Reynolds and Womersley numbers matched the physiological conditions. Nevertheless, the timing of flow jet would not be affected considerably by the change of viscosity. Our current study focuses on the angiographic evaluation so the aneurysmal wall thickness related to rupture risk is not considered. Introduction of a 6 F catheter (1.8 mm OD) increases the resistance of blood flow at the ICA. However, the diameter of the ICA at the cervical or petrous segment is 5mm so the catheter occupies less than 15% of the lumen and the effect of a catheter on the distal flow field is not significant. It is possible that the waveform distal to the catheter would be distorted but this effect applies to all three cases. Last, the current DSA will not be able to distinguish the flow jets at various phases of a cycle, but technological improvement on hardware would make the high frame rate DSA a useful clinical tool for intra-aneurysmal flow assessment in the future.

Conclusions

The timing of intra-aneurysmal flow jet depends on the contrast injection rate and aneurysm location. Visualization of flow jet at various phases of a cycle, except during the deceleration phase of the systole, is possible by varying the contrast injection rate. At an injection rate of 0.2 mL/s, flow jet on the DSA appears at the peak systole. The systolic flows for both the ICA and MCA aneurysms are better visualized with low injection rates (<0.5 mL/s), and the diastolic flow jets at the ICA aneurysms can be visualized with injection rates between 1 and 1.5 mL/s.

Acknowledgements

None.

Footnote

Conflicts of Interest: The authors have no conflicts of interest to declare.

References

1. Cebral JR, Raschi M. Suggested connections between risk factors of intracranial aneurysms: a review. Ann Biomed Eng 2013;41:1366-83.
2. Meng H, Tutino VM, Xiang J, Siddiqui A. High WSS or low WSS? Complex interactions of hemodynamics with intracranial aneurysm initiation, growth, and rupture: toward a unifying hypothesis. AJNR Am J Neuroradiol 2014;35:1254-62.
3. Sadasivan C, Fiorella DJ, Woo HH, Lieber BB. Physical factors effecting cerebral aneurysm pathophysiology. Ann Biomed Eng 2013;41:1347-65.
4. Brinjikji W, Cloft HJ, Fiorella D, Lanzino G, Kallmes DF. Estimating the proportion of intracranial aneurysms likely to be amenable to treatment with the pipeline embolization device. J Neurointerv Surg 2013;5:45-8.
5. Wakhloo AK, Gounis MJ. Revolution in aneurysm treatment: flow diversion to cure aneurysms: a paradigm shift. Neurosurgery 2014;61 Suppl 1:111-20.
6. Mut F, Raschi M, Scrivano E, Bleise C, Chudyk J, Ceratto R, Lylyk P, Cebral JR. Association between hemodynamic conditions and occlusion times after flow diversion in cerebral aneurysms. J Neurointerv Surg 2015;7:286-90.
7. Brinjikji W, Murad MH, Lanzino G, Cloft HJ, Kallmes DF. Endovascular treatment of intracranial aneurysms with flow diverters: a meta-analysis. Stroke 2013;44:442-7.
8. Fischer S, Vajda Z, Aguilar Perez M, Schmid E, Hopf N, Bäzner H, Henkes H. Pipeline embolization device (PED) for neurovascular reconstruction: initial experience in the treatment of 101 intracranial aneurysms and dissections. Neuroradiology 2012;54:369-82.
9. Piano M, Valvassori L, Quilici L, Pero G, Boccardi E. Midterm and long-term follow-up of cerebral aneurysms treated with flow diverter devices: a single-center experience. J Neurosurg 2013;118:408-16.
10. Grunwald IQ, Kamran M, Corkill RA, Kühn AL, Choi IS, Turnbull S, Dobson D, Fassbender K, Watson D, Gounis MJ. Simple measurement of aneurysm residual after treatment: the SMART scale for evaluation of intracranial aneurysms treated with flow diverters. Acta Neurochir (Wien) 2012;154:21-6; discussion 26.
11. Pereira VM, Bonnefous O, Ouared R, Brina O, Stawiaski J, Aerts H, Ruijters D, Narata AP, Bijlenga P, Schaller K, Lovblad KO. A DSA-based method using contrast-motion estimation for the assessment of the intra-aneurysmal flow changes induced by flow-diverter stents. AJNR Am J Neuroradiol 2013;34:808-15.
12. Sadasivan C, Cesar L, Seong J, Wakhloo AK, Lieber BB. Treatment of rabbit elastase-induced aneurysm models by flow diverters: development of quantifiable indexes of device performance using digital subtraction angiography. IEEE Trans Med Imaging 2009;28:1117-25.
13. Bonnefous O, Pereira VM, Ouared R, Brina O, Aerts H, Hermans R, van Nijnatten F, Stawiaski J, Ruijters D. Quantification of arterial flow using digital subtraction angiography. Med Phys 2012;39:6264-75.
14. Jou LD, Mawad ME. Analysis of intra-aneurysmal flow for cerebral aneurysms with cerebral angiography. AJNR Am J Neuroradiol 2012;33:1679-84.
15. Cebral JR, Mut F, Weir J, Putman CM. Association of hemodynamic characteristics and cerebral aneurysm rupture. AJNR Am J Neuroradiol 2011;32:264-70.
16. Tateshima S, Murayama Y, Villablanca JP, Morino T, Takahashi H, Yamauchi T, Tanishita K, Vinuela F. Intraaneurysmal flow dynamics study featuring an acrylic aneurysm model manufactured using a computerized tomography angiogram as a mold. J Neurosurg 2001;95:1020-7.
17. Tsai W, Savaş O. Flow pumping system for physiological waveforms. Med Biol Eng Comput 2010;48:197-201.
18. Zhang Y, Chong W, Qian Y. Investigation of intracranial aneurysm hemodynamics following flow diverter stent treatment. Med Eng Phys 2013;35:608-15.
19. Kulcsár Z, Augsburger L, Reymond P, Pereira VM, Hirsch S, Mallik AS, Millar J, Wetzel SG, Wanke I, Rüfenacht DA. Flow diversion treatment: intra-aneurismal blood flow velocity and WSS reduction are parameters to predict aneurysm thrombosis. Acta Neurochir (Wien) 2012;154:1827-34.
20. Chong W, Zhang Y, Qian Y, Lai L, Parker G, Mitchell K. Computational hemodynamics analysis of intracranial aneurysms treated with flow diverters: correlation with clinical outcomes. AJNR Am J Neuroradiol 2014;35:136-42.
21. Cebral JR, Mut F, Raschi M, Scrivano E, Ceratto R, Lylyk P, Putman CM. Aneurysm rupture following treatment with flow-diverting stents: computational hemodynamics analysis of treatment. AJNR Am J Neuroradiol 2011;32:27-33.
22. Benz T, Kowarschik M, Endres J, Redel T, Demirci S, Navab N. A Fourier-based approach to the angiographic assessment of flow diverter efficacy in the treatment of cerebral aneurysms. IEEE Trans Med Imaging 2014;33:1788-802.
23. Ford MD, Stuhne GR, Nikolov HN, Habets DF, Lownie SP, Holdsworth DW, Steinman DA. Virtual angiography for visualization and validation of computational models

of aneurysm hemodynamics. IEEE Trans Med Imaging 2005;24:1586-92.
24. Cebral JR, Pergolizzi RS Jr, Putman CM. Computational fluid dynamics modeling of intracranial aneurysms: qualitative comparison with cerebral angiography. Acad Radiol 2007;14:804-13.
25. Lieber BB, Sadasivan C, Hao Q, Seong J, Cesar L. The mixability of angiographic contrast with arterial blood. Med Phys 2009;36:5064-78.

Cite this article as: Jou L, Desai VR, Britz GW. *In vitro* investigation of contrast flow jet timing in patient-specific intracranial aneurysms. Quant Imaging Med Surg 2016;6(2):134-143. doi: 10.21037/qims.2016.03.06

